Expression, Two-Dimensional Crystallization, and Electron Cryo-crystallography of Recombinant Gap Junction Membrane Channels

Vinzenz M. Unger,*,[1] Nalin M. Kumar,* Norton B. Gilula,* and Mark Yeager*,†,[2]

*Department of Cell Biology, The Scripps Research Institute, 10550 North Torrey Pines Road, La Jolla, California 92037;
and †Division of Cardiovascular Diseases, Scripps Clinic, 10666 North Torrey Pines Road, La Jolla, California 92037

We used electron cryo-microscopy and image analysis to examine frozen-hydrated, two-dimensional (2D) crystals of a recombinant, 30-kDa C-terminal truncation mutant of the cardiac gap junction channel formed by 43-kDa α_1 connexin. To our knowledge this is the first example of a structural analysis of a membrane protein that has been accomplished using microgram amounts of starting material. The recombinant α_1 connexin was expressed in a stably transfected line of baby hamster kidney cells and spontaneously assembled gap junction plaques. Detergent treatment with Tween 20 and 1,2-diheptanoyl-*sn*-phosphocholine resulted in well-ordered 2D crystals. A three-dimensional density (3D) map with an in-plane resolution of ~7.5 Å revealed that each hexameric connexon was formed by 24 closely packed rods of density, consistent with an α-helical conformation for the four transmembrane domains of each connexin subunit. In the extracellular gap the aqueous channel was bounded by a continuous wall of protein that formed a tight electrical and chemical seal to exclude exchange of substances with the extracellular milieu. © 1999 Academic Press

Key Words: α_1 connexin; connexin43; gap junctions; intercellular communication; integral membrane proteins; electron cryo-microscopy; image analysis

INTRODUCTION

Gap junction membrane channels provide an intercellular pathway for passive diffusion of ions, metabolites, and molecules up to ~1000 Da (Loewenstein, 1981), thereby coordinating the metabolic and electrical activities of tissues. Previous low-resolution analyses of gap junction structure by X-ray scattering (Makowski *et al.,* 1977) and electron microscopy (Unwin and Ennis, 1984) supported a model in which the intercellular channel is formed by the end-to-end association of two oligomers termed connexons. More recently, recombinant DNA technology revealed the existence of a diverse multigene family of gap junction membrane proteins termed connexins (reviewed by Beyer *et al.,* 1990; Willecke *et al.,* 1991; Kumar and Gilula, 1992, 1996; Bruzzone *et al.,* 1996; Goodenough *et al.,* 1996). Experiments using protease cleavage, immunolabeling, and hydropathy analysis contributed to current models in which each connexin subunit traverses the membrane bilayer four times, placing the N- and C-termini on the cytoplasmic membrane surface (reviewed by Yeager and Nicholson, 1996; Yeager, 1998). Electron cryo-crystallography of a recombinant, C-terminal truncation mutant of 43-kDa α_1 cardiac connexin (α_1[Cx43])[3] has enabled us to derive two-dimensional (2D) and three-dimensional (3D) maps that confirm this model and show that each connexon is formed by 24 closely packed α-helices (Unger *et al.,* 1997, 1999).

EXPRESSION OF FULL-LENGTH AND C-TERMINAL TRUNCATED α_1 CONNEXIN IN BHK CELLS

A major challenge in the structure analysis of low-abundance polytopic integral membrane proteins has been the overexpression of sufficient functional material. A powerful approach for the electrophysiological characterization of gap junction channels has been provided by the expression of connexins and formation of functional channels in a variety of cell types such as *Xenopus* oocytes (Dahl *et al.,* 1987; Swenson *et al.,* 1989; Suchyna *et al.,* 1993; White *et al.,* 1995; Morley *et al.,* 1996; Oh *et al.,* 1997; Cao *et al.,* 1998) and transfected, communication-deficient mammalian cell lines [for example, SKHep1

cells (Eghbali *et al.,* 1990; Fishman *et al.,* 1990, 1991; Moreno *et al.,* 1991a,b), HeLa cells (Traub *et al.,* 1994; Verselis *et al.,* 1994; Elfgang *et al.,* 1995; Cao *et al.,* 1998), and mouse N2a neuroblastoma cells (Veenstra *et al.,* 1994, 1995; Beblo *et al.,* 1995; Brink *et al.,* 1997)]. However, the low level of expression in these systems precludes biochemical isolation and structural characterization. Connexins have been overexpressed in SF9 insect cells infected with a baculovirus vector (Stauffer *et al.,* 1991). However, high-resolution crystals could not be generated. By use of a stably transfected baby hamster kidney (BHK) cell line, connexins have been expressed under control of the inducible mouse metallothionein promoter by the addition of 100 µM zinc acetate to the culture medium (Fig. 1; Kumar *et al.,* 1995). Although the level of expression was quite low, the structure analysis was nevertheless feasible with just microgram amounts of recombinant material because the gap junction channels aggregate into plaques that can be isolated by cell fractionation techniques.

THE EXPRESSED RECOMBINANT CONNEXINS ASSEMBLE GAP JUNCTION PLAQUES

In BHK cells transfected with either the full-length or the C-terminal truncated α_1 connexin cDNA (α_1Cx-263T), indirect immunofluorescence microscopy showed that the antigen was localized to the cell surface as well as to intracellular sites (Fig.
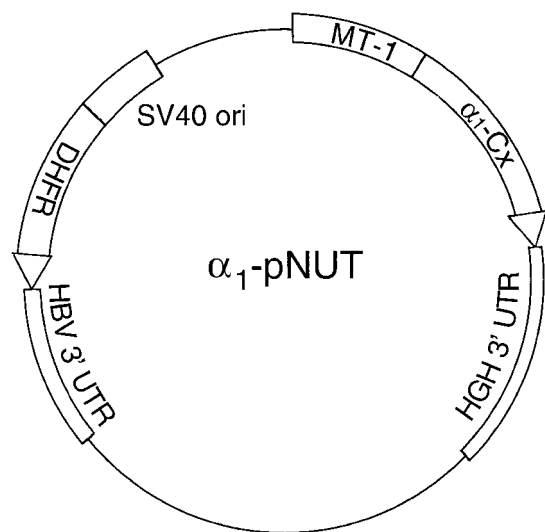
FIG. 1. Schematic of pNUT vector containing the rat heart α_1 connexin cDNA. The α_1 Cx cDNA was inserted between the mouse metallothionein promoter (MT-1) and the polyadenylation sequence of human growth hormone (HGH 3′UTR). Selection was based on the use of the dihydrofolate reductase gene (DHFR), which contained the polyadenylation site of the surface antigen gene from hepatitis B virus (HBV 3′UTR) and was under control of an SV40 promoter (SV40 ori) (Simonsen and Levinson, 1983; Palmiter *et al.,* 1987). Adapted from Kumar *et al.* (1995).

2). The punctate fluorescence on the cell surface was consistent with the assembly of the recombinant protein into gap junction plaques. By freeze-fracture analysis, plaques of variable size were detected with closely packed particles on the P fracture face and complementary pits on the E fracture face (Fig. 3). The gap junctions observed in BHK cells expressing α_1Cx-263T had a freeze-fracture morphology similar to that observed with BHK cells transfected with the full-length α_1 connexin cDNA. Taken together, the freeze-fracture and immunofluorescence results demonstrated that at least some of the recombinant α_1 connexin molecules were targeted to the plasma membrane and assembled into bona fide gap junctions.

IN SITU TWO-DIMENSIONAL CRYSTALLIZATION OF RECOMBINANT GAP JUNCTIONS

2D crystallization of membrane proteins is usually accomplished by reconstitution in which detergent-solubilized lipids are mixed with the detergent-solubilized and purified protein, and the detergent is removed by dialysis (Kühlbrandt, 1992; Jap *et al.,* 1992; Engel *et al.,* 1992). Gap junctions are formed by the aggregation of hundreds of channels in plaques that can be isolated by cell fractionation and sucrose gradient centrifugation. Since the protein is never removed from its native membrane, we refer to this approach as *in situ* crystallization (Yeager, 1994; Yeager *et al.,* 1999). Detergent extraction removes lipids to concentrate the gap junction channels in the plane of the membrane to generate a tightly packed lattice. Optical diffraction patterns of the best 2D crystals often showed sharp spots to better than 10-Å resolution (Unger *et al.,* 1997). A special advantage of such an expression system is the opportunity to generate mutants for detailed structure–function analysis. In order to focus on the transmembrane and extracellular architecture of the channel, the first mutant that we have examined, designated α_1Cx-263T, lacks most of the C-terminal domain of α_1[Cx43].

FACTORS INVOLVED IN THE IMPROVEMENT IN RESOLUTION OF THE 2D CRYSTALS

Electron microscopy and image analysis of native gap junctions isolated from heart (Yeager and Gilula, 1992), liver (Makowski *et al.,* 1977; Unwin and Ennis, 1984), and lens (Lampe *et al.,* 1991) have been limited to 15- to 20-Å resolution. Examination of biological specimens in the frozen-hydrated state offers the possibility of higher resolution structure analysis. However, the best resolution achieved in the analysis of frozen-hydrated liver gap junctions was also ~15 Å (Unwin and Ennis, 1984; Gogol and Unwin, 1988). Our ability to record data to higher
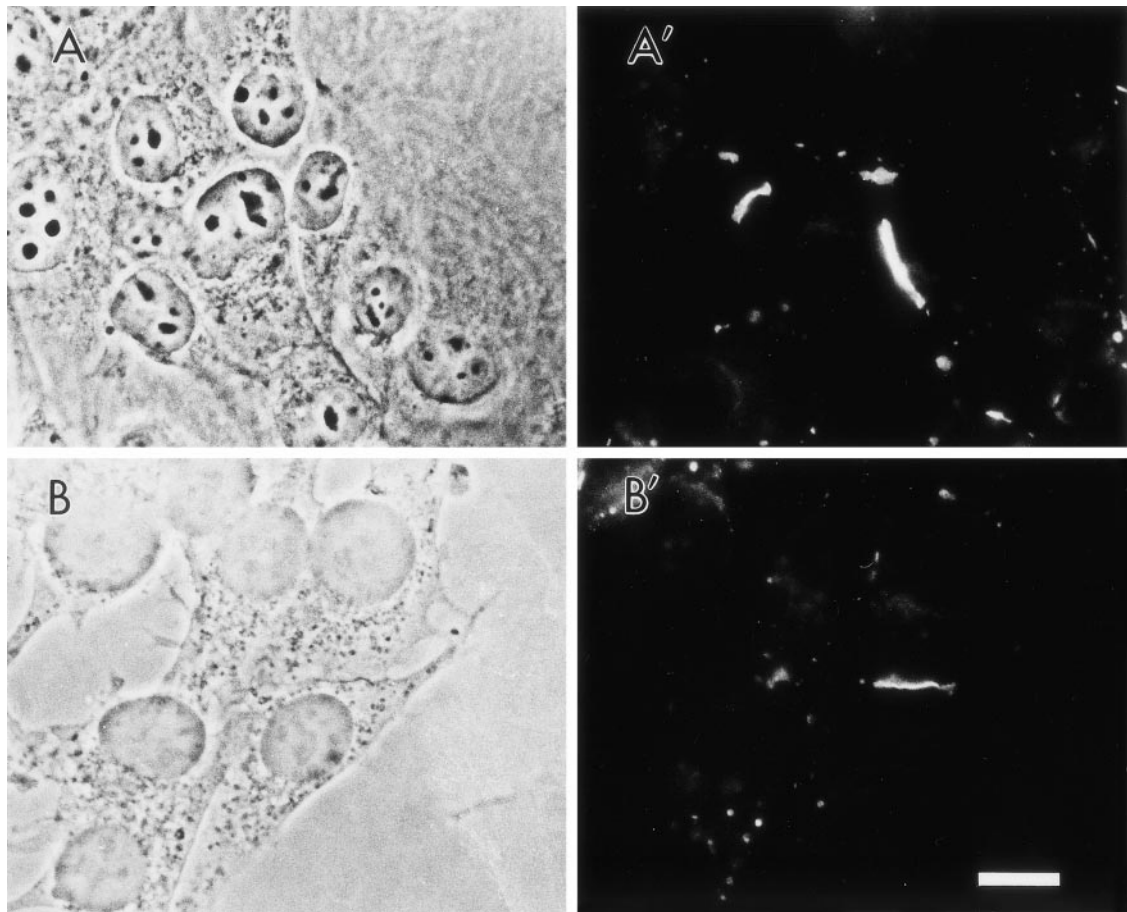
FIG. 2. Phase-contrast (left) and indirect immunofluorescence micrographs (right) of BHK cells transfected with the full-length (A and A′) or truncated α_1 connexin (α_1Cx-263T) cDNA (B and B′). Note the abundance of gap junction antigen on the cell surface at sites of intercellular contact, as well as in undefined intracellular sites. BHK cells were grown on glass coverslips and processed as previously described (Brissette *et al.,* 1994; Kumar *et al.,* 1995) using affinity-purified, polyclonal antibodies generated against a peptide corresponding to residues 131–142 in α_1[Cx43] (Yeager and Gilula, 1992). A Zeiss Axiophot was used for immunofluorescence microscopy. Bar represents 7.5 μm.

resolution from frozen-hydrated, recombinant gap junction channels was probably dependent on several factors that included the following.

(1) *Molecular homogeneity.* Liver tissue (Nicholson *et al.,* 1987) and cardiac tissue (Kanter *et al.,* 1992) are known to contain multiple connexin subtypes, which may be present in the same gap junction plaque. A special advantage of the stably transfected BHK cells is that only a specific connexin subtype is expressed. Although BHK cells naturally express full-length α_1[Cx43], Western immunoblots showed that the full-length protein was detected at only very low levels in overexposed immunoblots. Notably, the carboxy-tail in native cardiac gap junctions is sensitive to proteolysis (Manjunath *et al.,* 1985; Yeager and Gilula, 1992). By removing this protease-sensitive site in the mutant, the specimen was engineered to be more homogeneous.

(2) *2D crystallization.* In previous studies of liver

and heart gap junctions, *in situ* 2D crystallization was performed by treatment of gap junction plaques with lubrol (Zampighi and Unwin, 1979), deoxycholate (Zampighi and Unwin, 1979; Yeager, 1994), and dodecylmaltoside (Gogol and Unwin, 1988; Yeager, 1994). For the recombinant gap junctions, the variables that were tested to improve crystallinity included detergent screens (Tween 20, Tween 80, Tween 85, and cymol), chaotropes (potassium iodide and sodium thiosulfate), temperature (25 and 37°C), and incubation in glycerol. The Tween detergents were tested on the basis of their success in growing 2D crystals of frog rhodopsin (Schertler and Hargrave, 1995). If the potassium iodide treatment was not included, then the detergent extraction was not as successful. In addition, potassium iodide could not be replaced with sodium chloride. Best results were obtained by adjusting the protein concentration to 1 mg/ml and incubating the membrane suspension in
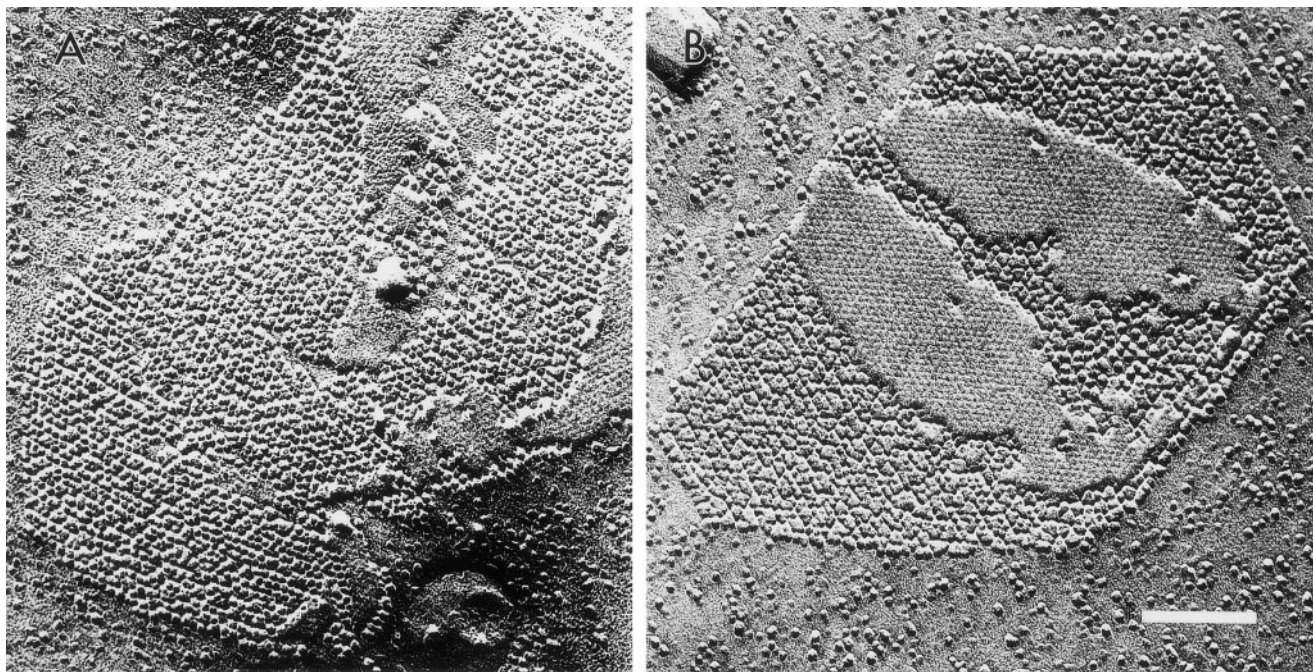
FIG. 3. Electron micrographs of freeze-fractured BHK cells expressing either full-length (left) or truncated α_1Cx-263T connexin (right). Both replicas display plaques that exhibit particles on the P fracture face and corresponding depressions on the E face that are typical of mammalian gap junctions. The plaque from the cells expressing α_1Cx-263T appears to be more crystalline than that from the cells expressing full-length α_1 [Gx43]. Cells were grown on plastic petri dishes and processed for freeze-fracture analysis as previously described (Kumar *et al.,* 1995). Freeze-fracture replicas were examined with a Hitachi H600 electron microscope at an accelerating voltage of 75 kV. Bar represents 200 nm.

2.8% Tween 20, 200 mM KI, 2 mM sodium thiosulfate, 140 µg/ml phenylmethylsulfonyl fluoride, 50 µg/ml gentamycin in 10 mM Hepes buffer (pH 7.5) containing 0.8% NaCl for 12 h at 27°C, followed by the addition of 1,2-diheptanoyl-*sn*-phosphocholine (DHPC) to 13 mg/ml and incubation for an additional 1 h at 27°C.

(3) *Electron cryo-microscopy*. The thermal stability and vibrational stability of cryo-microscopes have certainly improved over the past decade. For the projection density map, a resolution of 7 Å was achieved using a conventional Philips CM12 electron microscope operating at 100 kV, which was equipped with a standard Gatan626 cryo-stage (Unger *et al.,* 1997). For the 3D map, images of tilted crystals were recorded using a Philips 200-kV electron microscope equipped with a field emission 9 um. The improved stability and coherence of the 200-kV microscope compared with the CM12 was important for recording high-resolution images of tilted crystals. Nevertheless, high-resolution images could not be recorded from specimens tilted >35°. Factors that limit the resolution of images of tilted crystals include specimen flatness, beam-induced movement, and charging. The same 200-kV microscope and cold stage were used to collect higher resolution images of 2D crystals of AQP1 tilted to ~50° (Cheng *et al.,*

1997). Since the thickness of the AQP1 and gap junction crystals was ~60 and ~150 Å, respectively, we presume that the inability to record high-resolution images from highly tilted gap junction crystals was related to the increased thickness of the gap junction specimens.

(4) *Image processing*. The MRC image-processing package developed by R. Henderson and colleagues (Henderson *et al.,* 1986, 1990; Crowther *et al.,* 1996) was used to analyze the images and to correct for lattice distortions and effects of the contrast transfer function. Although lattice unbending has previously been used for the analysis of endogenous gap junctions (Gogol and Unwin, 1988; Yeager and Gilula, 1992), the MRC software has undergone substantial improvements compared with the earlier versions of the program. In particular, the program MAKETRAN was used to calculate a theoretical reference area based on the initial 3D density map of the structure, which improved the accuracy of the cross-correlation and unbending procedures.

Factors that probably did not significantly affect the improvement in resolution included the following.

(1) *Crystal size*. The isolated gap junction plaques were formed by a mosaic of crystalline areas. This mosaiacity as well as possible curvature of the

plaques made it necessary to use areas with only a few hundred unit cells for image processing. The small size of the crystals was comparable to crystals derived from liver and heart tissue. At present, the crystals are still too small for electron diffraction.

(2) *Specimen purity.* The gap junction preparations were substantially contaminated by nonjunctional membranes and were probably comparable in purity to crude plasma membrane preparations derived from liver tissue (Sikerwar and Unwin, 1988). DHPC treatment was particularly useful for solubilizing nonjunctional membranes. Nevertheless, SDS gels of the enriched membrane preparations displayed a pattern of bands that was similar to that of crude preparations. Even in the enriched specimens, a Coomassie-stainable band that corresponded to the recombinant gap junction protein was not detectable. The yield of gap junctions was quite variable from preparation to preparation. Nevertheless, the crystals were quite reproducible with a variation in unit cell size of 76 to 79 Å. These observations suggest that the major limiting factors in producing crystals was the culturing of the BHK cells and expression of recombinant protein. In general, if negatively stained specimens showed at least five crystals per grid square, then frozen-hydrated specimens were prepared. Since specimens that had more than five crystals per grid square were rarely produced, the major limiting factors for the cryomicroscopy were the number of crystals on the grid as well as the difficulty of recording images from tilted crystals.

α-HELICAL SECONDARY STRUCTURE OF RECOMBINANT GAP JUNCTIONS

The most prominent features in the two-dimensional projection density map were two concentric rings of six circular densities (Unger *et al.,* 1997). The circular densities at a radius of 17 Å from the central sixfold axis of symmetry lined the lumen of the central aqueous pore, whereas the densities at 33 Å were on the perimeter of the channel in contact with membrane lipids. These circular densities had the characteristic appearance of transmembrane α-helices oriented roughly perpendicular to the membrane plane (Unwin and Henderson, 1975; Kühlbrandt and Downing, 1989; Havelka *et al.,* 1993; Schertler *et al.,* 1993; Jap and Li, 1995; Karrasch *et al.,* 1995; Mitra *et al.,* 1995; Walz *et al.,* 1995; Hebert *et al.,* 1997). The two rings of α-helices were separated by a continuous band of density at a radius of 25 Å, which arose from the superposition of projections of additional transmembrane α-helices and polypeptide density arising from the extracellular and cytoplasmic loops within each connexin subunit.

THE DODECAMERIC CHANNEL IS FORMED BY 48 TRANSMEMBRANE α-HELICES

Image analysis of tilted 2D crystals yielded a 3D map with resolution cut-offs of 7.5 Å in the *x,y* plane and 21 Å along the *z* plane (Unger *et al.,* 1999). A side view of the map (Fig. 4) showed that the channel formed by the C-terminal truncation mutant had a thickness of ~150 Å, which compared with ~250 Å for gap junction channels formed by full-length α_1[Cx43] (Yeager, 1998). The reduced length of the recombinant channel is consistent with the loss of the ~13-kDa cytoplasmic C-tail.

In the 3D map, regions corresponding to the transmembrane (M) and extracellular (E) portions of the molecule were clearly resolved (Fig. 4). The outer diameter within the membrane region was ~70 Å, and the diameter narrowed to ~55 Å within the extracellular gap (Fig. 4A). A vertically sectioned view of the map (Fig. 4B) showed that the aqueous channel narrowed from ~40 to ~15 Å in proceeding from the cytoplasmic to the extracellular side of the bilayer. Within the hydrophobic regions of the bilayers, map sections displayed roughly circular contours of density that are typical for α-helices preferentially aligned perpendicular to the membrane (Fig. 4C, top and bottom). Since there are 24 circular densities per connexon, the dodecameric channel is formed by 48 transmembrane α-helices.

MODELS FOR THE DOCKING OF CONNEXONS

The extracellular region of the map was double-layered with a continuous band of density at ~17-Å radius and six arcs of density at ~26-Å radius (Fig. 4C, middle). The extracellular density was in distinct contrast to the characteristic "signature" for α-helices in cross section (Fig. 4C, top and bottom). This difference indicated that at least a portion of the polypeptide within the extracellular gap was not folded as α-helices. In fact, site-specific mutagenesis of the extracellular loops suggests that the polypeptide in the extracellular loops may fold as β-sheets (Foote *et al.,* 1998). The interior band of density formed a continuous wall of protein (Fig. 4B) that would serve as a tight electrical and chemical seal connecting the two cells.

A notable feature of the projection density map was the 30° displacement between the rings of α-helices at 17- and 33-Å radius, which places constraints on possible structural models for the intercellular channel. Assuming a roughly circular shape for the connexin subunit, the 30° displacement predicted that the two connexons forming the channel were likely to be rotationally staggered with respect to each other (Unger *et al.,* 1997; Perkins *et al.,* 1998). Because the connecting loops between the transmembrane α-helices were not revealed in the
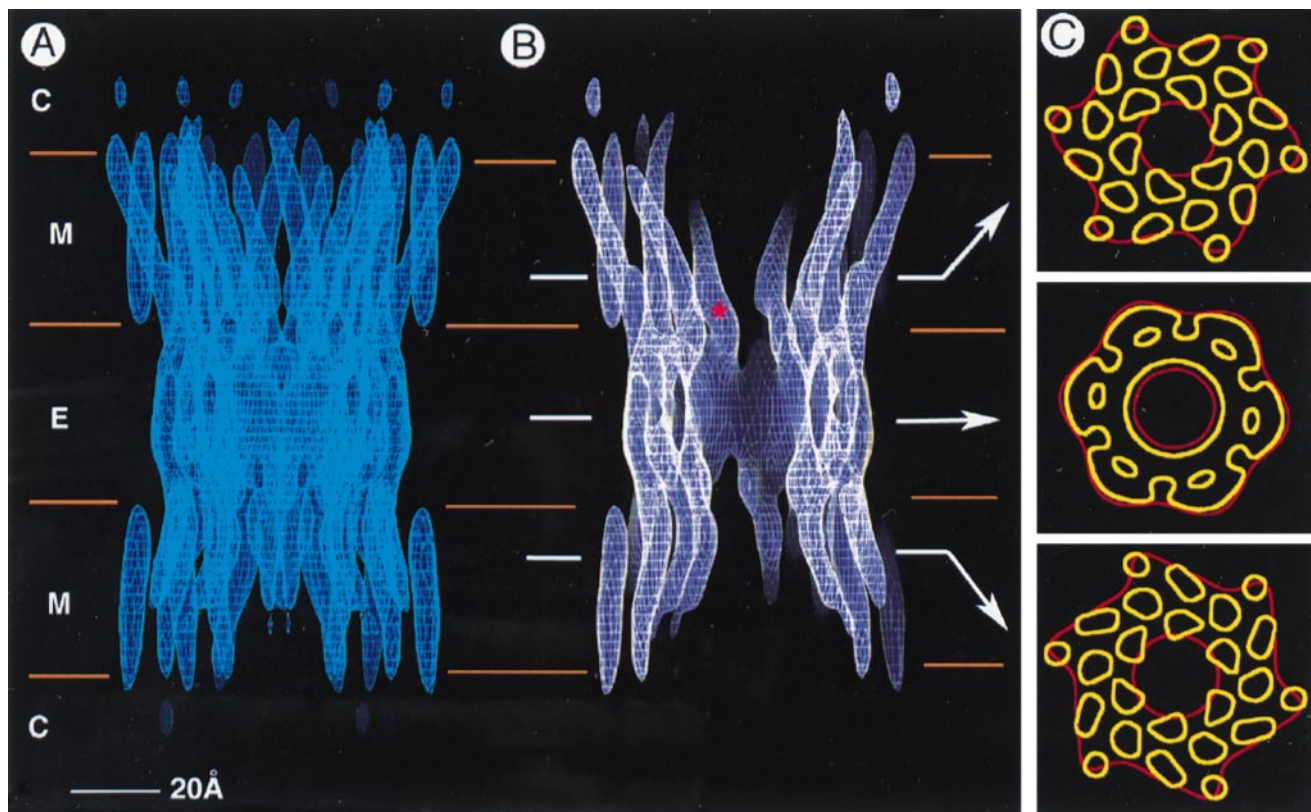
FIG. 4. Molecular organization of a recombinant gap junction channel. (A) A full side view is shown, and (B) the density has been cropped to show the channel interior. The approximate boundaries for the membrane bilayers (M), extracellular gap (E), and the cytoplasmic space (C) are indicated. The white arrows identify the locations of (C) the cross sections that are parallel to the membrane bilayers. The red contours in (C) are at 1σ above the mean density and include data to a resolution of 15 Å. These contours define the boundary of the connexon and can be compared to previous low-resolution structural studies of liver (Makowski *et al.,* 1977; Unwin and Ennis, 1984) and heart (Yeager and Gilula, 1992) gap junctions. The yellow contours at 1.5σ above the mean density include data to a resolution of 7.5 Å. The roughly circular shape of these contours within the hydrophobic region of the bilayers is consistent with 24 transmembrane α-helices per connexon. The maps in (A) and (B) were contoured at 3σ above the mean, which tends to eliminate density that is less well defined. The red asterisk in (B) marks the narrowest part of the channel where the aqueous pore is ~15 Å in diameter, not accounting for the contribution of amino acid side chains that are not resolved at the current limit of resolution. Electron cryo-microscopy and image analysis were performed as described. Reprinted with permission from Unger, V. M., Kumar, N. M., Gilula, N. B., and Yeager, M. Three-dimensional structure of a recombinant gap junction membrane channel, *Science* **283,** 1176–1180. Copyright 1999 American Association for the Advancement of Science.

3D map, there was ambiguity in assigning the molecular boundary of the connexin subunit. The 3D map was nevertheless consistent with reasonable models that involved rotational stagger, but some possible molecular boundaries did not involve rotational stagger. It is noteworthy that models with rotational stagger predict that each subunit in one connexon will interact with two connexin subunits in the apposing connexon. Such an arrangement may confer stability in the docking of the connexons.

FUTURE PROSPECTS

Higher resolution analysis is required to test the prediction that there is rotational stagger between the connexons. Other structural features yet to be determined are the molecular boundary and the assignment of the transmembrane α-helices to the four hydrophobic domains. In addition, a higher resolution map will reveal details about the folding and potential interactions of the extracellular loops that may provide insight into the high degree of stability between the docked connexons as well as how the extracellular loops confer selectivity in the docking process.

Preliminary functional studies of BHK cells that express α_1Cx-263T demonstrate that oleamide, a sleep-inducing compound, blocks *in vivo* dye transfer. As previously demonstrated for other connexins (Guan *et al.,* 1997), this behavior is an indication that oleamide causes closure of α_1Cx-263T. These results have encouraged us to compare the 3D structure of channels grown in the presence and in the absence of oleamide, which may allow us to explore the conformational changes that are associ-

ated with oleamide-induced blockage of dye transfer. The structural details revealed by our analysis will be essential for delineating the functional properties of this important class of channel proteins.

REFERENCES

Beblo, D. A., Wang, H.-Z., Beyer, E. C., Westphale, E. M., and Veenstra, R. D. (1995) Unique conductance, gating, and selective permeability properties of gap junction channels formed by connexin40, *Circ. Res.* **77,** 813–822.

Beyer, E. C., Paul, D. L., and Goodenough, D. A. (1990) Connexin family of gap junction proteins, *J. Membr. Biol.* **116,** 187–194.

Brink, P. R., Cronin, K., Banach, K., Peterson, E., Westphale, E. M., Seul, K. H., Ramanan, S. V., and Beyer, E. C. (1997) Evidence for heteromeric gap junction channels formed from rat connexin43 and human connexin37, *Am. J. Physiol.* **273,** C1386–C1396.

Brissette, J. L., Kumar, N. M., Gilula, N. B., Hall, J. E., and Dotto, G. P. (1994) Switch in gap junction protein expression is associated with selective changes in junctional permeability during keratinocyte differentiation, *Proc. Natl. Acad. Sci. USA* **91,** 6453–6457.

Bruzzone, R., White, T. W., and Paul, D. L. (1996) Connections with connexins: The molecular basis of direct intercellular signalling, *Eur. J. Biochem.* **238,** 1–27.

Calero, G., Kanemitsu, M., Taffet, S. M., Lau, A. F., and Delmar, M. (1998) A 17mer peptide interferes with acidification-induced uncoupling of connexin43, *Circ. Res.* **82,** 929–935.

Cao, F., Eckert, R., Elfgang, C., Nitsche, J. M., Snyder, S. A., Hülser, D. F., Willecke, K., and Nicholson, B. J. (1998) A quantitative analysis of connexin-specific permeability differences of gap junctions expressed in HeLa transfectants and *Xenopus* oocytes, *J. Cell Sci.* **111,** 31–43.

Cheng, A., van Hoek, A. N., Yeager, M., Verkman, A. S., and Mitra, A. K. (1997) Three-dimensional organization of a human water channel, *Nature* **387,** 627–630.

Crowther, R. A., Henderson, R., and Smith, J. M. (1996) MRC image processing programs, *J. Struct. Biol.* **116,** 9–16.

Dahl, G., Miller, T., Paul, D., Voellmy, R., and Werner, R. (1987) Expression of functional cell–cell channels from cloned rat liver gap junction complementary DNA, *Science* **236,** 1290–1293.

Eghbali, B., Kessler, J. A., and Spray, D. C. (1990) Expression of gap junction channels in communication-incompetent cells after stable transfection with cDNA encoding connexin 32, *Proc. Natl. Acad. Sci. USA* **87,** 1328–1331.

Elfgang, C., Eckert, R., Lichtenberg-Fraté, H., Butterweck, A., Traub, O., Klein, R. A., Hülser, D. F., and Willecke, K. (1995) Specific permeability and selective formation of gap junction channels in connexin-transfected HeLa cells, *J. Cell Biol.* **129,** 805–817.

Engel, A., Hoenger, A., Hefti, A., Henn, C., Ford, R. C., Kistler, J., and Zulauf, M. (1992) Assembly of 2-D membrane protein crystals: Dynamics, crystal order, and fidelity of structure analysis by electron microscopy, *J. Struct. Biol.* **109,** 219–234.

Fishman, G. I., Moreno, A. P., Spray, D. C., and Leinwand, L. A.

(1991) Functional analysis of human cardiac gap junction channel mutants, *Proc. Natl. Acad. Sci. USA* **88,** 3525–3529.

Fishman, G. I., Spray, D. C., and Leinwand, L. A. (1990) Molecular characterization and functional expression of the human cardiac gap junction channel, *J. Cell Biol.* **111,** 589–598.

Foote, C. I., Zhou, L., Zhu, X., and Nicholson, B. J. (1998) The pattern of disulfide linkages in the extracellular loop regions of connexin 32 suggests a model for the docking interface of gap junctions, *J. Cell Biol.* **140,** 1187–1197.

Gogol, E., and Unwin, N. (1988) Organization of connexons in isolated rat liver gap junctions, *Biophys. J.* **54,** 105–112.

Goodenough, D. A., Goliger, J. A., and Paul, D. L. (1996) Connexins, connexons, and intercellular communication, *Annu. Rev. Biochem.* **65,** 475–502.

Guan, X., Cravatt, B. F., Ehring, G. R., Hall, J. E., Boger, D. L., Lerner, R. A., and Gilula, N. B. (1997) The sleep-inducing lipid oleamide deconvolutes gap junction communication and calcium wave transmission in glial cells, *J. Cell Biol.* **139,** 1785–1792.

Havelka, W. A., Henderson, R., Heymann, J. A. W., and Oesterhelt, D. (1993) Projection structure of halorhodopsin from *Halobacterium halobium* at 6Å resolution obtained by electron cryo-microscopy, *J. Mol. Biol.* **234,** 837–846.

Hebert, H., Schmidt-Krey, I., Morgenstern, R., Murata, K., Hirai, T., Mitsuoka, K., and Fujiyoshi, Y. (1997) The 3.0Å projection structure of microsomal glutathione transferase as determined by electron crystallography of $p2_12_12$ two-dimensional crystals, *J. Mol. Biol.* **271,** 751–758.

Henderson, R., Baldwin, J. M., Downing, K. H., Lepault, J., and Zemlin, F. (1986) Structure of purple membrane from Halobacterium halobium: Recording, measurement and evaluation of electron micrographs at 3.5Å resolution, *Ultramicroscopy* **19,** 147–178.

Henderson, R., Baldwin, J. M., Ceska, T. A., Zemlin, F., Beckmann, E., and Downing, K. H. (1990) Model for the structure of bacteriorhodopsin based on high-resolution electron cryo-microscopy, *J. Mol. Biol.* **213,** 899–929.

Homma, N., Alvarado, J. L., Coombs, W., Stergiopoulos, K., Taffet, S. M., Lau, A. F., and Delmar, M. (1998) A particle-receptor model for the insulin-induced closure of connexin43 channels, *Circ. Res.* **83,** 27–32.

Jap, B. K., and Li, H. (1995) Structure of the osmo-regulated H_2O-channel, AQP-CHIP, in projection at 3.5Å resolution, *J. Mol. Biol.* **251,** 413–420.

Jap, B. K., Zulauf, M., Scheybani, T., Hefti, A., Baumeister, W., Aebi, U., and Engel, A. (1992) 2D crystallization: From art to science, *Ultramicroscopy* **46,** 45–84.

Kanter, H. L., Saffitz, J. E., and Beyer, E. C. (1992) Cardiac myocytes express multiple gap junction proteins, *Circ. Res.* **70,** 438–444.

Karrasch, S., Bullough, P. A., and Ghosh, R. (1995) The 8.5Å projection map of the light-harvesting complex I from *Rhodospirillum rubrum* reveals a ring composed of 16 subunits, *EMBO J.* **14,** 631–638.

Kühlbrandt, W. (1992) Two-dimensional crystallization of membrane proteins, *Q. Rev. Biophys.* **25,** 1–49.

Kühlbrandt, W., and Downing, K. H. (1989) Two-dimensional structure of plant light-harvesting complex at 3.7Å resolution by electron crystallography, *J. Mol. Biol.* **207,** 823–828.

Kumar, N. M., Friend, D. S., and Gilula, N. B. (1995) Synthesis and assembly of human β_1 gap junctions in BHK cells by DNA transfection with the human β_1 cDNA. *J. Cell Sci.* **108,** 3725–3734.

Kumar, N. M., and Gilula, N. B. (1992) Molecular biology and genetics of gap junction channels, *Semin. Cell Biol.* **3,** 3–16.

Kumar, N. M., and Gilula, N. B. (1996) The gap junction communication channel, *Cell* **84,** 381–388.

Lampe, P. D., Kistler, J., Hefti, A., Bond, J., Müller, S., Johnson, R. G., and Engel, A. (1991) *In vitro* assembly of gap junctions, *J. Struct. Biol.* **107,** 281–290.

Liu, S., Taffet, S., Stoner, L., Delmar, M., Vallano, M. L., and Jalife, J. (1993) A structural basis for the unequal sensitivity of the major cardiac and liver gap junctions to intracellular acidification: The carboxyl tail length, *Biophys. J.* **64,** 1422–1433.

Loewenstein, W. R. (1981) Junctional intercellular communication: The cell-to-cell membrane channel, *Physiol. Rev.* **61,** 829–913.

Makowski, L., Caspar, D. L. D., Phillips, W. C., and Goodenough, D. A. (1977) Gap junction structures. II. Analysis of the X-ray diffraction data, *J. Cell Biol.* **74,** 629–645.

Manjunath, C. K., Goings, G. E., and Page, E. (1985) Proteolysis of cardiac gap junctions during their isolation from rat hearts, *J. Membr. Biol.* **85,** 159–168.

Mitra, A. K., van Hoek, A. N., Wiener, M. C., Verkman, A. S., and Yeager, M. (1995) The CHIP28 water channel visualized in ice by electron crystallography, *Nat. Struct. Biol.* **2,** 726–729.

Moreno, A. P., Eghbali, B., and Spray, D. C. (1991a) Connexin32 gap junction channels in stably transfected cells: Unitary conductance, *Biophys. J.* **60,** 1254–1266.

Moreno, A. P., Eghbali, B., and Spray, D. C. (1991b) Connexin32 gap junction channels in stably transfected cells. Equilibrium and kinetic properties, *Biophys. J.* **60,** 1267–1277.

Morley, G. E., Taffet, S. M., and Delmar, M. (1996) Intramolecular interactions mediate pH regulation of connexin43 channels, *Biophys. J.* **70,** 1294–1302.

Nicholson, B., Dermietzel, R., Teplow, D., Traub, O., Willecke, K., and Revel, J.-P. (1987) Two homologous protein components of hepatic gap junctions, *Nature* **329,** 732–734.

Oh, S., Ri, Y., Bennett, M. V. L., Trexler, E. B., Verselis, V. K., and Bargiello, T. A. (1997) Changes in permeability caused by connexin 32 mutations underlie X-linked Charcot–Marie–Tooth disease, *Neuron* **19,** 927–938.

Palmiter, R. D., Behringer, R. R., Quaife, C. J., Maxwell, F., Maxwell, I. H., and Brinster, R. L. (1987) Cell lineage ablation in transgenic mice by cell-specific expression of a toxic gene, *Cell* **50,** 435–443.

Perkins, G. A., Goodenough, D. A., and Sosinsky, G. E. (1998) Formation of the gap junction intercellular channel requires a 30° rotation for interdigitating two apposing connexons, *J. Mol. Biol.* **277,** 171–177.

Rubin, J. B., Verselis, V. K., Bennett, M. V. L., and Bargiello, T. A. (1992) A domain substitution procedure and its use to analyze voltage dependence of homotypic gap junctions formed by connexins 26 and 32, *Proc. Natl. Acad. Sci. USA* **89,** 3820–3824.

Schertler, G. F. X., Villa, C., and Henderson, R. (1993) Projection structure of rhodopsin, *Nature* **362,** 770–772.

Schertler, G. F. X., and Hargrave, P. A. (1995) Projection structure of frog rhodopsin in two crystal forms, *Proc. Natl. Acad. Sci. USA,* **92,** 11578–11582.

Sikerwar, S. S., and Unwin, N. (1988) Three-dimensional structure of gap junctions in fragmented plasma membranes from rat liver, *Biophys. J.* **54,** 113–119.

Simonsen, C. C., and Levinson, A. D. (1983) Isolation and expression of an altered mouse dihydrofolate reductase cDNA, *Proc. Natl. Acad. Sci. USA* **80,** 2495–2499.

Stauffer, K. A., Kumar, N. M., Gilula, N. B., and Unwin, N. (1991) Isolation and purification of gap junction channels, *J. Cell Biol.* **115,** 141–150.

Suchyna, T. M., Xu, L. X., Gao, F., Fourtner, C. R., and Nicholson, B. J. (1993) Identification of a proline residue as a transduction element involved in voltage gating of gap junctions, *Nature* **365,** 847–849.

Swenson, K. I., Jordan, J. R., Beyer, E. C., and Paul, D. L. (1989) Formation of gap junctions by expression of connexins in Xenopus oocyte pairs, *Cell* **57,** 145–155.

Traub, O., Eckert, R., Lichtenberg-Fraté, H., Elfgang, C., Bastide, B., Scheidtmann, K. H., Hülser, D. F., and Willecke, K. (1994) Immunochemical and electrophysiological characterization of murine connexin40 and -43 in mouse tissues and transfected human cells, *Eur. J. Cell Biol.* **64,** 101–112.

Unger, V. M., Kumar, N. M., Gilula, N. B., and Yeager, M. (1997) Projection structure of a gap junction membrane channel at 7Å resolution, *Nat. Struct. Biol.* **4,** 39–43.

Unger, V. M., Kumar, N. M., Gilula, N. B., and Yeager, M. (1999) Three-dimensional structure of a recombinant gap junction membrane channel, *Science* **283,** 1176–1180.

Unwin, P. N. T., and Ennis, P. D. (1984) Two configurations of a channel-forming membrane protein, *Nature* **307,** 609–613.

Unwin, P. N. T., and Henderson, R. (1975) Molecular structure determination by electron microscopy of unstained crystalline specimens, *J. Mol. Biol.* **94,** 425–440.

Veenstra, R. D., Wang, H.-Z., Beyer, E. C., and Brink, P. R. (1994) Selective dye and ionic permeability of gap junction channels formed by connexin45, *Circ. Res.* **75,** 483–490.

Veenstra, R. D., Wang, H.-Z., Beblo, D. A., Chilton, M. G., Harris, A. L., Beyer, E. C., and Brink, P. R. (1995) Selectivity of connexin-specific gap junctions does not correlate with channel conductance, *Circ. Res.* **77,** 1156–1165.

Verselis, V. K., Ginter, C. S., and Bargiello, T. A. (1994) Opposite voltage gating polarities of two closely related connexins, *Nature* **368,** 348–354.

Walz, T., Typke, D., Smith, B. L., Agre, P., and Engel, A. (1995) Projection map of aquaporin-1 determined by electron crystallography, *Nat. Struct. Biol.* **2,** 730–732.

White, T. W., Paul, D. L., Goodenough, D. A., and Bruzzone, R. (1995) Functional analysis of selective interactions among rodent connexins, *Mol. Biol. Cell* **6,** 459–470.

Willecke, K., Hennemann, H., Dahl, E., Jungbluth, S., and Heynkes, R. (1991) The diversity of connexin genes encoding gap junctional proteins, *Eur. J. Cell Biol.* **56,** 1–7.

Yeager, M. (1994) *In situ* two-dimensional crystallization of a polytopic membrane protein: The cardiac gap junction channel, *Acta. Crystallogr. Sect. D* **50,** 632–638.

Yeager, M. (1998) Structure of cardiac gap junction intercellular channels, *J. Struct. Biol.* **121,** 231–245.

Yeager, M., and Gilula, N. B. (1992) Membrane topology and quaternary structure of cardiac gap junction ion channels, *J. Mol. Biol.* **223,** 929–948.

Yeager, M., and Nicholson, B. J. (1996) Structure of gap junction intercellular channels, *Curr. Opin. Struct. Biol.* **6,** 183–192.

Yeager, M., Unger, V. M., and Mitra, A. K. (1999) Three-dimensional structure of membrane proteins determined by two-dimensional crystallization, electron cryomicroscopy, and image analysis, *Methods Enzymol.* **294,** 135–180.

Zampighi, G., and Unwin, P. N. T. (1979) Two forms of isolated gap junctions, *J. Mol. Biol.* **135,** 451–464.